

Elastic stiffness constants of copper indium diselenide determined by neutron scattering

René Fouret

Laboratoire de Dynamique et Structure des Matériaux Moléculaires, Université de Lille I, 59655 Villeneuve d'Ascq CEDEX, France

Bernard Hennion

Laboratoire Léon Brillouin, Centre d'Etudes Nucléaires de Saclay, 91191 Gif-sur-Yvette, France

J. Gonzalez and S. M. Wasim

Centro de Estudios de Semiconductores, Facultad de Ciencias, Universidad de los Andes, Merida 5101 Venezuela

(Received 19 May 1992; revised manuscript received 11 December 1992)

From the acoustic-dispersion curves determined by inelastic neutron scattering, we obtain at room temperature the elastic stiffness constants of CuInSe_2 : at 10^{10} Nm^{-1} , $c_{11}=9.70$, $c_{12}=5.97$, $c_{13}=8.60$, $c_{33}=10.89$, and $c_{44}=3.62$. A theoretical calculation based upon the sphalerite approximation gives good agreement with the values of c_{11} and c_{44} . Using the elastic constants, the isothermal compressibility is calculated along the c axis and the ab plane. Two low-energy optical modes were also observed at frequencies near 55 cm^{-1} at the Brillouin-zone center.

The ternary compound CuInSe_2 (CIS) of the I-III-VI₂ family has received considerable attention in recent years because of its potential for applications in solar cell devices.¹ It crystallizes in the chalcopyrite structure ($I\bar{4}2d$) (Ref. 2) shown in Fig. 1 with the lattice parameters $a = 5.782 \text{ \AA}$ and $c = 11.620 \text{ \AA}$.

Although the literature abounds with data on the electrical,³⁻⁵ optical,^{6,7} and thermal properties^{8,9} of this compound, only a limited number of papers related to the lattice vibrational studies have been reported^{8,10-12} and data on the acoustic modes of this compound have not been reported at all to our knowledge. However, the knowledge of elastic characteristics and low-energy opti-

cal modes would allow the analysis of the temperature dependence of the specific heat, thermal expansion, and Grüneisen constants and would provide information to the study of interatomic and anharmonic effects which are of great interest for device fabrication.

In the present work, we report on the dispersion curves of acoustic and low-energy optical phonons and the elastic constants of CIS obtained from inelastic neutron scattering at 300 K on a single crystal of 0.12 cm^3 produced by horizontal Bridgman technique.¹³ The elastic constants and compressibility, deduced from these measurements, will be compared with those calculated from the extended Keating model.^{14,15}

Inelastic neutron experiments were performed at room temperature and atmospheric pressure at the Orphée reactor (Laboratoire Léon Brillouin, Saclay) on a triple-axis spectrometer 1T installed on a thermal source. Both monochromator and the analyzer were pyrolytic graphite in (002) reflection. The horizontal collimators were $30^\circ\text{-}40^\circ\text{-}60^\circ\text{-}60^\circ$ or $30^\circ\text{-}40^\circ\text{-}40^\circ\text{-}40^\circ$ yielding an energy resolution of 0.25 or 0.20 THz full width at half maximum for neutrons of wave vector $k_i = 2.662 \text{ \AA}^{-1}$. Since the main objective of the experiment was to determine the elastic stiffness constants, we have measured the acoustic-phonon branches, in general along high-symmetry axes in the three scattering planes, namely the [001], [100], and [110]. For each phonon measured, the exact peak frequency was obtained by deconvoluting the measured intensity with the resolution function.

The measured acoustic and optical-phonon dispersion curves along [001], [110], and [100] are displayed on Figs. 2, 3, and 4. Other measurements have been performed along [101] and [111] directions to allow the determination of all the elastic constants. Furthermore, it was possible to record two optical branches $\text{TO}[001]$ and $\text{TO}_1[110]$ with the polarization vectors $e(110)$ and $e(010)$, respectively. In addition, the frequency of the $\text{TA}[001]$, $\text{TO}[001]$, $\text{TA}_1[110]$, $\text{TO}_1[110]$, $\text{TA}_1[100]$, and $\text{TA}_2[110]$

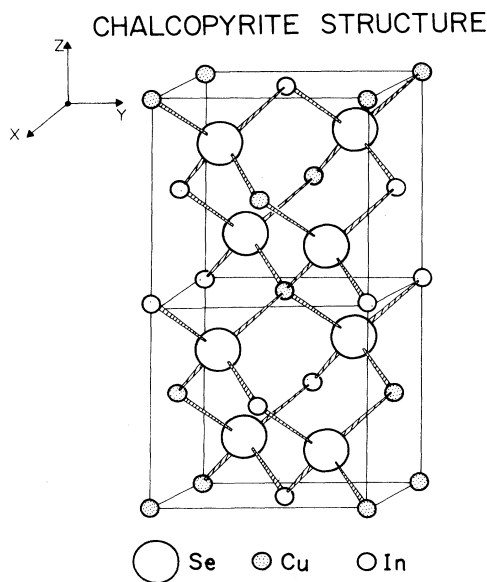


FIG. 1. Chalcopyrite structure of CuInSe_2 .

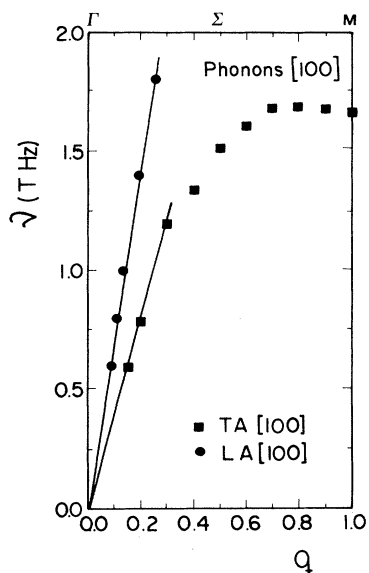


FIG. 2. Phonon dispersion curves of TA[100] and LA[100] modes of CuInSe₂. The units of the q sector are $2\pi/a$.

TABLE I. The transverse acoustic- and optical-modes frequencies of CuInSe₂ at the zone center and zone boundary.

	Zone center		Zone border	
	THz	cm ⁻¹	THz	cm ⁻¹
TA[001]			1.53	51
TO[001]	1.65	55	1.50	50
TA ₁ [110]			1.51	50.4
TO ₁ [110]	1.67	55.7	1.51	50.4
TA ₁ [100]			1.66	55.4
TA ₂ [110]			2.10	70

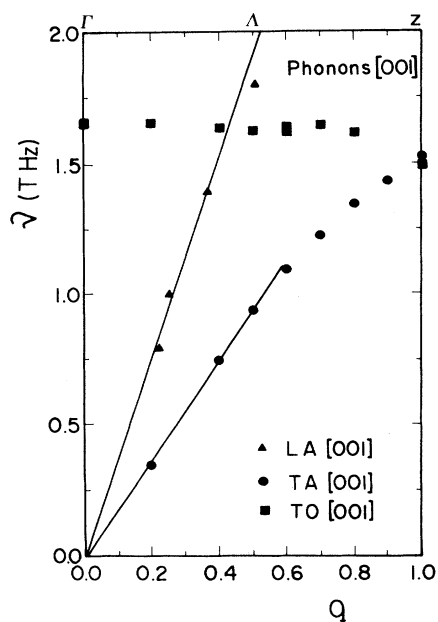


FIG. 3. Phonon dispersion curves of the LA[001], TA[001], and TO[001] modes of CuInSe₂. The units of the q vector are $2\pi/c$.

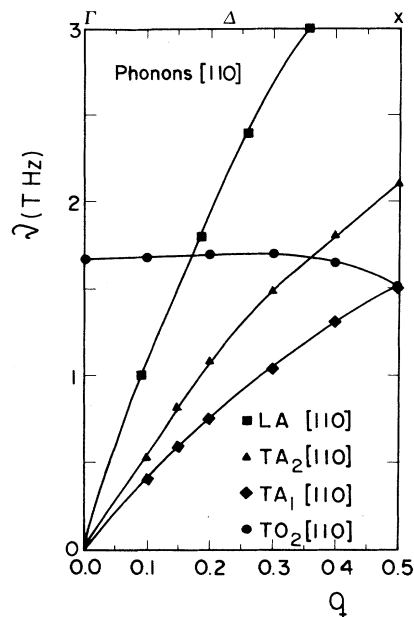


FIG. 4. Phonon dispersion curves of the TA₁[110], TA₂[110], LA[110], and TO₂[110] modes of CuInSe₂. The units of q are $2\pi\sqrt{2}/a$.

modes at the zone border were also measured. These are given in Table I.

It can be noticed that the dispersion curves reported on Figs. 2, 3, and 4 are quite similar to those already observed for ZnS, ZnSe, and ZnTe of the analog binary family II-VI.¹⁶ In particular, the phonon dispersion curve of the TA[100] mode of CIS (see Fig. 2) is very similar to that of TA (Γ -X) and TA (Γ -L) curve of the binary analog II-VI.^{16,17}

Defining $V(q)$ as $2\pi\nu/q$, where ν and q are the frequency and wave vector of a measured acoustic phonon, the sound velocity $V(0)$ will be obtained through the approximation

$$V(q) = V(0)(1 - \alpha q^2). \quad (1)$$

This is illustrated on Fig. 5 for a transverse mode along the [100] direction. The values of $V(0)$ thus determined

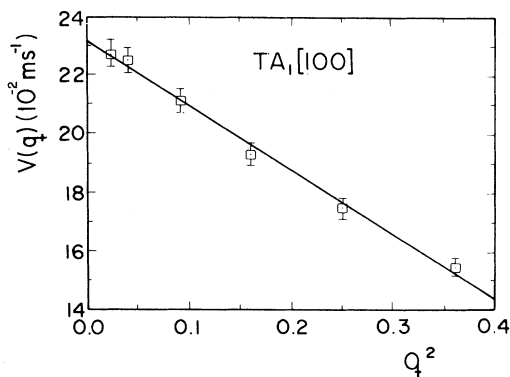


FIG. 5. Illustrative example of the calculation of the phonon velocity of the TA₁[110] mode using Eq. (1).

TABLE II. Experimentally extrapolated and calculated velocities of acoustic-phonon modes with different polarization vectors in CuInSe₂.

Phonon mode	Polarization vector	V (ms ⁻¹)	
		V(0) Experimental	V Calculated
LA[100]	[100]	4194	4108
TA ₁ [100]	[010]	2381	2344
TA ₂ [100]	[001]	2479	2510
LA[001]	[001]	4370	4371
TA[001]	[100]	2416	2510
LA[110]	[110]	4309	4373
TA ₁ [110]	[110]	1772	1801
TA ₂ [110]	[001]	2589	2510
LA[111]	[11u]	4514	4586
TA[111]	[-1-12u ⁻¹]	2213	2095
LA[101]	[10v]	4604	4560
TA[101]	[10-v ⁻¹]	1617	1682

are reported in Table II for 12 measured acoustic branches.

The expression of the velocities as a function of the elastic constants is given by the Christoffel equations,

$$(L_{ik} - \rho V^2 \delta_{ik}) U_k = 0, \quad i, k = 1, 2, 3, \quad (2)$$

where L_{ik} is the propagation matrix of the acoustic waves, and ρ the room-temperature density 5749 kg m⁻³ for CIS. U_1 , U_2 , and U_3 are the direction cosines of the particle displacement vectors. In the case of a tetragonal crystal the relation (2), applied to the 12 measured acoustic branches, provides 12 equations depending on the 6 elastic constants. A least-squares fitting routine was used to get the following set of values in units of 10¹⁰ Nm⁻¹: $c_{11} = 9.70$, $c_{12} = 5.97$, $c_{13} = 8.60$, $c_{33} = 10.89$, $c_{44} = 3.62$, and $c_{66} = 3.16$, where the standard deviation from the least-squares fit is within 5%. Furthermore, it can be pointed out that the relative magnitude of the c_{ij} 's satisfy the Born stability criteria,¹⁹ c_{11} , c_{33} , c_{44} , and $c_{66} > 0$; $c_{11} > |c_{12}|$; $c_{11}c_{33} > c_{13}^2$; and $(c_{11} + c_{12})c_{33} > 2c_{13}^2$ valid for a tetragonal structure of the chalcopyrite. The longitudinal and transverse velocities calculated with the fitted c_{ij} 's are reported in Table II, illustrating the good overall agreement with experiment.

TABLE III. Elastic constants from neutron experiments in CuInSe₂ and those calculated from the sphalerite approximation in 10¹⁰ Nm⁻¹ units. Reported data on the elastic constants of AgGaS₂ and CdGeAs₂ for comparison.

	Neutron data	Sphalerite model	Reported values	
			AgGaS ₂ ^a	CdGeAs ₂ ^b
C_{11}	9.70	8.07	8.79	9.45
C_{33}	10.89		7.58	8.34
C_{44}	3.62	3.22	2.41	4.21
C_{66}	3.16		3.08	4.08
C_{12}	5.97	5.00	5.84	5.96
C_{13}	8.60		5.92	5.97

^aSee Ref. 19.

^bSee Ref. 18.

TABLE IV. Reported values of the active infrared and Raman modes E , B_2^1 and E_3 , B_2^2 of AgInSe₂ and CuInSe₂ that are used to calculate the bond-bending and the bond-stretching force constants in CuInSe₂.

	AgInSe ₂ ^a		CuInSe ₂ ^b	
	ω_{TO} cm ⁻¹	ω_{LO} cm ⁻¹	ω_{TO} cm ⁻¹	ω_{LO} cm ⁻¹
III-V				
E_1	215	231	213	230
B_2^1	208	233	214	231
I-VI				
E_3			180	193
B_2^2			181	193

^aReference 20.

^bReference 12.

The set of elastic constants of CIS can be compared with those reported for AgGaS₂ (Ref. 19) and CdGeAs₂.¹⁸ We have as in AgGaS₂ and CdGeAs₂, shown in Table III, $c_{12} < c_{11}$ and $c_{12} < c_{33}$, but contrary to these compounds, in our case, we obtain $c_{11} < c_{33}$. No explanation of this behavior is possible at this stage.

It is well established that the active infrared and Raman modes E_1 and B_2^1 in the ternary compound semiconductors of the I-III-VI₂ family that have chalcopyrite structure are sphalerite in nature and are determined by the properties of the III-VI sublattice alone.¹⁰ The difference between the frequencies of these modes depends on bond-bending forces and is very small, as is their evolution small within a set of compounds having the same III-VI sublattice. This is illustrated in Table IV where are compared the data of the E_1 and B_2^1 modes of AgInSe₂ and CuInSe₂. Similar behavior is also expected for the E_3 and B_2^2 modes where the I-VI sublattice plays the decisive role.

Using the frequencies of Raman modes from Table IV, c , a , and the reported values d_{I-VI} , d_{III-VI} , and ϵ_∞ for CIS given in Table V, the bond-stretching and bond-bending force constants have been determined and reported in Table VI. For this, the Keating model extended by Martin¹⁵ for compounds with sphalerite structure was used. Using the values of the parameters given in Tables V and VI, the elastic constants c_{11} , c_{12} , and c_{44} are calculated. These are also given in Table III for comparison with the values obtained from inelastic neutron scattering. It can be observed that the calculated elastic constants c_{11} and c_{44} are in good agreement with those obtained from neutron-scattering data. From the relation $\chi_T = 3/(c_{11} + 2c_{12})$ the isothermal compressibility is cal-

TABLE V. Reported values used to calculate the elastic constants according to Martin (Ref. 15).

Interatomic distance ^a	Ionicity ^a	Dielectric constant ^b
$d_{I-VI} = 2.456 \text{ \AA}$	$f_{I-VI} = 0.77$	$\epsilon_\infty = 8.1$
$d_{III-VI} = 2.561 \text{ \AA}$	$f_{III-VI} = 0.60$	$\epsilon_0 = 13.6$

^aReference 2.

^bReference 4.

TABLE VI. Calculated values from Keating model as extended by Martin of the bond-bending and the bond-stretching force constants α and β (in N m^{-1}) and the dynamic effective charge Z^* in CuInSe_2 .

	CuInSe_2
$\alpha_{\text{I-VI}}$	26.9
$\alpha_{\text{III-VI}}$	43.6
$\beta_{\text{I-VI}}$	1.48
$\beta_{\text{III-VI}}$	4.47
$Z_{\text{I-VI}}^*$	0.88
$Z_{\text{III-VI}}^*$	1.3

culated under the sphalerite approximation. With the values of the elastic constants from the column 3 of Table III, we find this to be $1.61 \times 10^{-11} \text{ N}^{-1} \text{ m}^2$ which is in good agreement with the value of $1.62 \times 10^{-11} \text{ N}^{-1} \text{ m}^2$ reported in Ref. 8. However, the calculated c_{12} , although very close to that of ZnSe , is about 20% smaller than that of the neutron-scattering experiment. In the case of chalcopyrite structure, using the linear elasticity approximation,²¹ the compressibility can also be calculated directly from the elastic constants:

$$\chi_T = \chi_{T,c} + 2\chi_{T,ab}, \quad (3)$$

where $\chi_{T,c}$ and $\chi_{T,ab}$ are the compressibilities along the c axis and in the ab plane, respectively, of chalcopyrite structure. These two compressibilities are expressed as

$$\chi_{T,c} = (c_{11} + c_{12} - 2c_{13})/c, \quad (4)$$

$$\chi_{T,ab} = (c_{33} - c_{13})/c, \quad (5)$$

where $c = c_{33}(c_{11} + c_{12}) - 2c_{13}^2$.

With the values of our elastic constants obtained from the neutron-scattering experiments and Eqs. (4) and (5), we obtain $\chi_{T,c} = -2.57 \times 10^{-12} \text{ N}^{-1} \text{ m}^2$ and $\chi_{T,ab} = 7.70 \times 10^{-12} \text{ N}^{-1} \text{ m}^2$. This from Eq. (3) gives $\chi_T = 1.28 \times 10^{-11} \text{ N}^{-1} \text{ m}^2$. This value can be compared with $0.8 \times 10^{-11} \text{ N}^{-1} \text{ m}^2$ deduced from the Grüneisen parameter obtained from the thermal-conductivity measurements, $1.62 \times 10^{-11} \text{ N}^{-1} \text{ m}^2$ reported in Ref. 8, $2.07 \times 10^{-11} \text{ N}^{-1} \text{ m}^2$ obtained from ultrasonic measurements of the longitudinal and transverse sound velocities²² in polycrystalline samples, $2.38 \times 10^{-11} \text{ N}^{-1} \text{ m}^2$ from microhardness²³ in single crystals, and $1.61 \times 10^{-11} \text{ N}^{-1} \text{ m}^2$ calculated from the cubic approximation in the present work. Although a negative value of $\chi_{T,c}$ is physically not impossible, this point should be considered with caution. Indeed it should be emphasized that this negative value is essentially due to the large value found for c_{13} . Because of the expression of $\chi_{T,c}$ [Eq. (4)] the accuracy of the determination of $\chi_{T,c}$ may be affected by the correlations between the uncertainties on the fitted elastic constants more drastically than those only deduced from the standard errors.

In conclusion, our neutron inelastic measurements allowed the determination of the elastic constants of CuInSe_2 and thus provided the starting point of the study of the lattice dynamics of this compound. Measurements of optical-phonon branches are currently in progress.

This work was performed under the framework of a E.E.C., Contract No. CII-0556F. The Laboratoire de Dynamique et Structure des Matériaux Moléculaires is Unité Associée au CNRS No. 801.

- ¹A. Rockett and R. W. Birkmire, *J. Appl. Phys.* **70**, R81 (1991).
²J. E. Jaffe and A. Zunger, *Phys. Rev. B* **29**, 1882 (1984).
³T. Irie, S. Endo, and S. Kimura, *Jpn. J. Appl. Phys.* **18**, 1303 (1979).
⁴S. M. Wasim, *Solar Cells* **16**, 289 (1986).
⁵H. Neumann and R. D. Tomlinson, *Sol. Cells* **28**, 301 (1990).
⁶C. Rincon, J. Gonzalez, and G. Sanchez Perez, *Phys. Status Solidi B* **108**, K19 (1981).
⁷C. Rincon, C. Bellabarba, J. Gonzalez, and G. Sanchez Perez, *Sol. Cells* **16**, 335 (1986).
⁸H. Neumann, *Sol. Cells* **16**, 399 (1986).
⁹S. M. Wasim and A. Noguera, *Phys. Status Solidi A* **32**, 553 (1984).
¹⁰H. Neumann, *Helv. Phys. Acta* **58**, 337 (1985).
¹¹J. Gonzalez, M. Quintero, and C. Rincon, *Phys. Rev. B* **45**, 7022 (1992).
¹²J. Gonzalez and S. M. Wassim (unpublished).
¹³J. P. Peyrade, S. M. Wasim, F. Voillot, J. Leotin, and J. Gali-

- bert, (unpublished).
¹⁴P. N. Keating, *Phys. Rev.* **149**, 674 (1966).
¹⁵R. M. Martin, *Phys. Rev. B* **1**, 4005 (1970).
¹⁶D. N. Talwar, M. Vandevyver, K. Kunc, and M. Zigone, *Phys. Rev. B* **24**, 741 (1981).
¹⁷B. A. Weinstein, *Solid State Commun.* **24**, 595 (1977).
¹⁸Tu Hailing, G. A. Saunders, W. A. Lambson, and R. S. Fielgelson, *J. Phys. C* **15**, 1399 (1982).
¹⁹M. H. Grimsditch and G. D. Holah, *Phys. Rev. B* **12**, 4377 (1975).
²⁰G. Kannelis and K. Kampas, *Mater. Res. Bull.* **13**, 9 (1978).
²¹D. Vanne and C. Wallace, *Thermodynamics of Crystals* (Wiley, New York, 1972), pp. 32–41.
²²B. Fernandez and S. M. Wasim, *Phys. Status Solidi A* **122**, 235 (1990).
²³G. Constantinidis, R. D. Tomlinson, and H. Neumann, *Philos. Mag. Lett.* **57**, 91 (1988).